Published in final edited form as:
Cell Rep. 2013 October 17; 5(1): . doi:10.1016/j.celrep.2013.08.051.

The organization of submodality-specific touch afferent inputs in the vibrissa column

Katsuyasu Sakurai[1], **Masahiro Akiyama**[1,2], **Bin Cai**[3], **Alexandra Scott**[1], **Bao-Xia Han**[1], **Jun Takatoh**[1], **Markus Sigrist**[4], **Silvia Arber**[4], and **Fan Wang**[1,*]

[1]Department of Cell Biology, Box 3709, Duke University Medical Center, Durham, NC 27710 [2]Department of Physiological Chemistry, Graduate School of Comprehensive Human Sciences and Institute of Basic Medical Sciences, University of Tsukuba, 1-1-1 Ten-nohdai, Tsukuba 305-8571, Japan [3]Key Laboratory of Brain Functional Genomics, Institute of Cognitive Neuroscience, East China Normal University, 3663 North Zhongshan Road, Shanghai 200062, P.R. China [4]Biozentrum, Department of Cell Biology, University of Basel, 4056 Basel, and Friedrich Miescher Institute for Biomedical research, 4058 Basel, Switzerland

SUMMARY

The rodent tactile vibrissae are innervated by several different types of touch sensory neurons. The central afferents of all touch neurons from one vibrissa collectively project to a columnar structure called barrelette in brainstem. Delineating how distinct types of sensors connect to second-order neurons within each barrelette is critical for understanding tactile information coding and processing. Using genetic and viral techniques, we selectively labeled slowly-adapting (SA) mechanosensory neurons, rapidly-adapting (RA) mechanosensory neurons, afferent synapses, and second-order projection neurons with different “colors”, respectively, to examine the connectivity. We discovered that within each vibrissa column, individual sensory neurons project collaterals to multiple distributed locations; inputs from SA and RA afferents are spatially intermixed without any discernible stereotypy or topography; second-order projection neurons receive convergent SA and RA inputs. Our findings reveal a “one-to-many and many-to-one” connectivity scheme and the circuit architecture for tactile information processing at the first-order synapses.

INTRODUCTION

Humans use fingers to detect and discriminate diverse types of textures and forms in the natural and artificial world. Four types of touch receptor neurons are found in the glabrous skin of primate fingers: two slowly-adapting (Merkel disc and Ruffini endings) and two rapidly-adapting receptors (Pacinian corpuscles and Meissner’s corpuscles). However, the connectivity formed between these distinct types of touch neurons and the second-order neurons in the central nervous system (CNS) remains a mystery. Solving this connectivity puzzle is critical for understanding of how the nervous system encodes and discriminates diverse textures and forms.

[*]**Correspondence should be addressed to Fan Wang**, fan.wang@duke.edu, tel: 919-684-3682.

Here we examine this question using the rodent vibrissa sensory system as a model, which has tactile sensitivity comparable to that of primate fingertips (Carvell and Simons, 1990). Vibrissae are large facial hairs. Each is densely innervated by the peripheral axons of 100~200 trigeminal (TG) sensory neurons (Rice et al., 1986; Welker and Van der Loos, 1986). The central axons of these neurons project into the brainstem, and can collectively form a cylinder-like neural structure, called a barrelette. At the gross anatomical level, all vibrissae are precisely and topographically mapped onto multiple brain regions as a set of cylinder structures: barrelettes in the brainstem, barreloids in thalamus and barrels in cortex (Erzurumlu et al., 2010; Killackey et al., 1995; Woolsey and Van der Loos, 1970). These structures have been considered as the preeminent examples of “columnar organization” or “labeled-lines” of the nervous system. At the detailed anatomical level, TG neurons innervating a single vibrissa consist of six to seven distinct types, which presumably detect distinct features of mechanical stimuli elicited by vibrissa deflection, vibration or motion (Bosman et al., 2011; Ebara et al., 2002; Rice et al., 1997). However, it is unknown how different types of touch neurons (sub-modalities) organize their synaptic inputs within these “labeled-lines” or “columns”. In addition, TG neurons send collaterals into four brainstem nuclei: principalis (PrV), spinal oralis (SpO), interpolaris (SpI), and caudalis (SpC), and barrelette columns are found in three out of the four nuclei in PrV, SpI and SpC. It is unclear whether different brainstem nuclei employ the same or different principles in organizing TG afferents inside their corresponding barrelettes.

Different types of TG touch neurons form distinct specialized sensory endings inside each vibrissa follicular-sinus-complex (FSC). They are (from top to the base of the FSC): superficial Merkel endings at the rete ridge collar, transverse lanceolate endings at the level of the inner conical body, longitudinal lanceolate and deep Merkel endings at the level of the ring sinus, club-, spiny (Ruffini)-, and reticular-endings at the level of the cavernous sinus (Ebara et al., 2002; Hasegawa et al., 2007) (Fig. 1A). It is known that Merkel ending neurons are slowly-adapting (SA) and potentially signal ongoing stimulus, whereas the lanceolate-ending neurons are rapidly-adapting (RA) mechanosensors and presumably detect changes in stimulus (Gottschaldt et al., 1973; Li et al., 2011; Lumpkin et al., 2010). Moreover, SA neurons were found to respond more selectively than RA neurons to the direction of vibrissa movements (Lichtenstein et al., 1990). However, whether RA and SA inputs from TG neurons are spatially segregated within each barrelette into sub-columns in any of the brainstem nuclei (PrV, SpI or SpC) is unknown. Furthermore, whether second-order projection neurons receive selective (RA or SA only) or convergent (both RA and SA) inputs is also undetermined. To solve these basic connectivity questions, here we carried out studies using a combination of genetic and viral based circuit tracing techniques.

RESULTS

Genetic labeling of RA and SA TG touch neurons

We searched for molecular markers that may selectively label a specific type of trigeminal ganglion (TG) touch sensory neurons. Chondrolectin (Chodl) is a C-type lectin known to be expressed in muscle cells (Weng et al., 2003), fast motor neurons (Enjin et al., 2010) and subsets of sensory neurons in the dorsal root ganglion (DRG) (Allen Brain Atlas, http://www.brain-map.org/). We found that in TG, >96% of *Chodl* expressing neurons co-express *Ret* (Fig. 1D), i.e. they represent subsets of Ret+ sensory receptors. A knock-in mouse line was generated in which the human placenta alkaline phosphatase (PLAP) replaced the first exon of the *Chodl* gene ($Chodl^{PLAP/+}$) (fig. S1A–C, Fig.1B). PLAP-staining on mystacial pad sections revealed that inside the vibrissa follicles, the rapidly-adapting (RA) longitudinal lanceolate endings were selectively labeled (Fig. 1B). This is consistent with a previous finding showing that RA lanceolate-ending neurons express Ret (Luo et al., 2009). Further, *Chodl* is not expressed by second-order neurons in the brainstem nuclei (SpC, SpI,

SpO and PrV) (Allen Brain Atlas, http://www.brain-map.org/; and data not shown). Thus, we can use Chodl$^{PLAP/+}$ mice to visualize axonal projections from the longitudinal lanceolate RA neurons into the barrelette structures. Expression of *Chodl* is also observed in skin cells, in a small number of unmyelinated c-fiber neurons (~10% Chodl+ neurons do *not* express NF200 and thus are unmyelinated, fig. S1D), and in subpopulations of motor neurons (data not shown). Since these other expressions are not relevant to the study of the vibrissa barrelette circuit, they are not discussed further.

Our previous studies and other work suggested that parvalbumin may be another good candidate for labeling subtypes of touch receptor neurons (Hasegawa and Wang, 2008; Ichikawa and Sugimoto, 2003). To examine this possibility, we crossed the Pv::Cre knock-in mice (Hippenmeyer et al., 2005) with several Cre-dependent reporter lines (Rosa-loxP-STOP-loxP-PLAP, abbreviated as RΦAP; or Rosa-loxP-STOP-loxP-XFP, abbreviated as RΦGFP or RΦtomato mice) (Arenkiel et al., 2011; da Silva et al., 2011; Que et al., 2008). All reporter lines were generated in our lab using the same strategy and gave essentially similar labeling (for details, see Extended Experimental Procedures). Using the PLAP reporter (RΦAP), we found that in the adult mouse, Pv::Cre selectively labeled only two types of vibrissa neurons: SA Merkel-ending neurons and a small number of RA longitudinal lanceolate ending neurons (Fig. 1C). This is different from what has been known for DRG sensory neurons, of which most Pv+ cells are muscle spindle or Golgi tendon innervating proprioceptive neurons (Arber et al., 2000; Ernfors et al., 1994). This difference between TG and DRG is further evidenced by the expression of neurotrophin receptors. The majority of Pv+ DRG neurons co-express TrkC (Arber et al., 2000). By contrast, of the TG neurons labeled by Pv::Cre, 62% expresses TrkC, 17% co-expresses TrkA, while 26% co-localize with Ret (Fig. 1E, the total number exceeds 100%, implying that some neurons co-express two of the receptors). Although the *Pv* gene itself is known to express in second-order neurons in the brainstem trigeminal nuclei (Bennett-Clarke et al., 1992), the reporter expression in the brainstem was only observable beginning at around postnatal day 7 (P7). This provides us a window of opportunity to examine the axonal projection patterns from Pv-expressing TG neurons at P7~8 without the confounding of the neuronal processes from central neurons. At this neonatal age, more than 90% of Merkel cells in *smaller* vibrissae are innervated by axons labeled with Pv::Cre (Fig. 1F, upper panels); whereas in the *larger* vibrissae (those that are located more caudally), many fewer Merkel cells are innervated by Pv::Cre positive axons (Fig. 1F, lower panels).

We generated triple transgenic mice Pv::Cre; RΦtomato; Chodl$^{PLAP/+}$ (Fig. 1G). About 25% of Pv::Cre-labeled neurons (tomato fluorescent) co-express PLAP (Chodl^{PLAP}) in TG, consistent with the finding that 26% of Pv::Cre cells express Ret. Since Pv::Cre labels only longitudinal lanceolate- and Merkel-ending neurons, while Chodl^{PLAP} selectively labels lanceolate type neurons, it follows that ~25% of the Pv::Cre lineage cells are Ret/Chodl double positive RA-lanceolate neurons, while 75% of the Pv::Cre lineage cells are either TrkC and/or TrkA-expressing SA-Merkel ending neurons in TG. The tomato/PLAP double positive cells are about 22% of total Chodl+ (PLAP stained) neurons in TG.

Axon projections and synaptic maps of RA and SA afferents inside the brainstem

To examine how RA-lanceolate and SA-Merkel ending neurons organize their afferent inputs within the vibrissa-representing barrelettes, we serial sectioned the brains from Pv::Cre; RΦtomato; Chodl^{PLAP} triple transgenic mice (all at P7 stage), and simultaneously visualized tomato, PLAP, and vGluT1 (vesicular glutamate transporter 1) signals (Fig. 2, fig. S2). vGluT1 is expressed by all myelinated TG sensory neurons, as evidenced by the near complete co-localization of anti-vGluT1 and anti-NF200 staining signals (NF200 marks all myelinated neurons) (fig. S1E). Anti-vGluT1 stains touch afferent termini and thus also delineates the individual barrelette structures in the brainstem (Fig. 2A, 2C). Both Pv-tomato

(red) and Chodl-PLAP (green) axons were observed in all brainstem trigeminal nuclei (Fig. 2A, 2C, fig. S2A), suggesting that as populations, both types (SA-Merkel and RA-lanceolate) of touch sensors provide inputs to all 4 nuclei. Pv-tomato signals appeared concentrated in "smaller" barrelettes. This was expected, as Pv::Cre mediated reporter expression labeled most of the Merkel ending neurons in smaller but not larger vibrissae at this P7 stage (Fig. 1F). In these smaller barrelettes, the axonal projections from both populations of neurons overlap extensively, with no apparent spatial segregation within the barrelettes in both SpI (Fig. 2A) and PrV (Fig. 2C).

We next examined whether the SA-Merkel and RA-lanceolate axons form *synapses* in spatially stereotyped locations within each barrelette. To visualize the distributions of the lanceolate presynaptic termini, we extracted out the sites where PLAP (RA-axons) and vGluT1 (presynaptic sites) signals co-localized in the Z-stacks from each of the serial sections throughout an entire barrelette, and these lanceolate synaptic sites were pseudo-colored "green" (fig. S2B). Similarly, we extracted tomato and vGluT1 double-positive sites from the same Z-stacks of each of the serial sections (fig. S2C), and these were considered as presynaptic termini from both Merkel- and a subset of lanceolate-ending neurons. Consistently, the tomato+/vGluT1+ and PLAP+/vGluT1+ synaptic sites were largely non-overlapping. The overlapping portions, which were tomato/PLAP/vGluT1 triple-positive sites, were roughly 25% of the total tomato+/vGluT1+ spots (data not shown). Therefore, from the total tomato+/vGluT1+ sites, we deleted those tomato/PLAP/vGluT1 triple-positive spots, and obtained Merkel-ending specific presynaptic termini that were pseudo-colored "red" (fig. S2D). Through such analyses, we were able to generate "synapses distribution maps" for both RA-lanceolate and SA-Merkel afferents within individual barrelettes (Fig. 2B, 2D, fig. S3). As examples of synapse distribution maps where nearly *all* SA-Merkel-endings were labeled, we analyzed the barrelettes representing the small D6 whisker in different mice (n=7 small barrelettes, Fig. 2B, 2D and data not shown). In addition, we also analyzed large barrelettes in which Merkel-ending afferents were only partial or sparsely labeled at this age (n=8 large barrelettes, fig. S3 and data not shown).

Figure 2B and 2D show the maps of RA-lanceolate (green) and SA-Merkel (red) presynaptic sites in the D6 barrelette from 3 different animals in SpI (Fig. 2B) or PrV (Fig. 2D) nucleus. To give a general idea of the distributions, presynaptic sites extracted from the Z-stacks of all 6 serial sections are shown. Blue dots on each image are vGluT1 only spots that represent presynaptic sites from other unlabeled types of touch-sensory neurons, and/or vGluT1-positive termini from CNS neurons (Fig. 2B and 2D). For 3D views of the synapse maps for each of the serial sections (reconstructed combining all the z-stacks per section), please see representative movies (suppl. movie M1 and M2). On all sections, synapses formed by RA-lanceolate and SA-Merkel afferents are spatially interspersed, displaying a mosaic pattern in both SpI and PrV (Fig. 2B and 2D, fig. S3, movie M1 and M2). In the larger barrelettes, although Merkel-synapses (red) are only sparsely labeled, they are nevertheless spatially intermingled with lanceolate-synapses (green), and the lanceolate-synapses themselves are also distributed throughout these large barrelettes in both SpI and PrV nuclei with a "salt-and-pepper" pattern (fig. S3).

Notably, the distributions are not even, with certain regions/sections containing more synapses, while other regions/sections containing many fewer RA- or SA-synapses. This "unevenness" was already apparent from the axonal projections where axon arbors often did not cover the whole area of a barrelette but rather concentrated into patches (arrows in Fig. 2A and 2C). To quantitatively describe such "uneven" distributions, we aligned the serial sections together (combining z-stacks from all sections of the barrelette) and computed the *relative* synaptic densities for RA-lanceolate or SA-Merkel-synapses and expressed the results as "heatmaps" (see Experimental Procedures for details). For visualization, the 3D

synapse density heatmaps were projected onto three 2D planes (illustrated in fig. S3A): coronal (C), lateral/sagittal (L), or horizontal (H) planes for RA- and SA-afferent synapses, respectively. These 2D-heatmaps are shown next to the serial section images (right panels in Fig. 2B, 2D, fig. S3C, S3D).

The heatmaps reveal four features of RA- and SA-synapse distributions. First, both RAand SA-synapses are distributed and there is no clear topographic segregation of the two submodality-specific inputs. Second, there are scattered “hot spots” (red colored) and “cold spots” (dark-blue) for both RA- and SA-inputs, revealing the “unevenness” of their synaptic distributions. Third, the heatmaps for RA- and SA-synapses vary significantly among different barrelettes and among the same barrelettes of different animals. Finally, there are no discernible stereotypical locations for the hot- or cold-spots for either RA- or SA-synapses, even when comparing the same D6 barrelette from different animals. The lack of stereotypy is further supported by cross-correlation analysis of SA- and RA-synapse maps in the D6 barrelettes from 4 different animals (fig. S3B). Very low or no correlations was detected between SA- and RA- synapse maps within the same animals, or between SA- and/or RA-synapses among different animals (fig. S3B). These results together indicate that RA- and SA-touch afferent inputs do not segregate into any ordered sub-columns within an individual vibrissa column, and on the whole, RA- or SA-synapses are unevenly and highly variably distributed throughout the column.

Single neuron provides divergent and distributed inputs into the vibrissa column

We next examined the axon collateral projections from a single RA lanceolate- or a single SA Merkel-ending neuron inside individual vibrissa columns using Pv::CreERt2 knock-in mice, in which the tamoxifen-inducible CreERt2 was expressed under the control of the *Pv* gene (see Experimental Procedures). In Pv::CreERt2; RΦtomato mice, one-time low dose tamoxifen injection in neonatal pups (≤P5) activated CreERt2 activity and induced permanent tomato expression in small number of Pv-expressing TG neurons (Fig. 3A). Sectioning through the mystacial pads allowed identification of those vibrissae in which only a single sensory neuron (single axon plus terminal endings) was labeled (Fig. 3B). Since 75% of Pv-expressing neurons are Merkel ending type and the other 25% of Pv-neurons are lanceolate type, single-labeled lanceolate neurons were recovered at lower frequency using this strategy. We serial sectioned through the brainstems to visualize the axon collateral arborization patterns originating from a single neuron at two developmental stages P8 and P28. This is because our population analyses described above were performed at P7, and it is possible that connectivity patterns might change as the animals mature. Thus, we wanted to examine whether the axon arborization patterns observed in young mice were similar to those in mature animals (P28), hence whether the organizations uncovered at P7 also apply to the adult mice.

An example of such serial sections showing the single-labeled neuron elaborating multiple axonal collaterals through a barrelette in SpI is shown in fig. S4A. All sections were co-stained with anti-vGluT1 to delineate the boundaries of the barrelettes (yellow outlines). After centered alignment of the serial sections, 3D reconstructions of the axon arbors in the corresponding barrelette were performed for both SpI and PrV nuclei. Fig. 3C shows the coronal, and lateral views of collaterals from one representative Merkel- (Fig. 3C1, 3C3) or one lanceolate-ending neurons (Fig. 3C2, 3C4) inside the corresponding barrelette column in SpI (upper panels) and in PrV (lower panels) at both P8 (Fig. 3C1, 3C2) and P28 (Fig. 3C3, 3C4) stages. The 3D-rotating views of the reconstructed arbors from both types of neurons in the two nuclei are shown in supplemental movies M3–M6. Additional examples of such reconstructions (from both ages) are shown in Supplemental fig. S4.

These reconstructions revealed that individual lanceolate or Merkel ending neurons project multiple distributed axonal collaterals inside the barrelette column in both SpI and PrV (Fig. 3, fig. S4, movies M3–M6). The arbors of the collaterals are largely confined within the barrelette boundary. However, the number, size and spatial distribution of the collaterals in each barrelette are not fixed (e.g. in Fig. 3C1, the labeled Merkel-neuron projected sparsely in the PrV barrelette, but densely in the SpI barrelette). Importantly, collaterals are similarly elaborated and distributed throughout the barrelette column at both P8 and P28. We measured the normalized volume occupied by collaterals from individual neurons (see Experimental Procedures) and found no statistically significant differences between P8 and P28 stage for both types of afferents (Fig. 3D). Furthermore, using co-localization with vGluT1 (fig. S4C), we quantified the number of synapses formed by single neurons and then normalized to the volume of the collaterals to assess relative synapse densities. The normalized synaptic densities of single RA- or SA- afferents do not differ significantly between P8 and P28 stages (Fig. 3E). These results support the idea that touch sensory axon arborizations show mature patterns at around 1-week of age and there is no extensive pruning as the animal further develops. This is consistent with previous findings regarding collateral aborizations of DRG sensory neurons in the spinal cord, that axon arborization patterns displayed at P7 were the same as those in adult (Woodbury and Koerber, 2007; Woodbury et al., 2001). All single-labeled neurons also projected collaterals into SpO and SpC nuclei (data not shown), consistent with previous single neuron studies using tracers such as HRP that found an average of 12~16 collaterals per neuron throughout the entire brainstem (Hayashi, 1985; Jacquin et al., 1993; Jacquin et al., 1988; Jacquin et al., 1986). Taken together, our analysis showed that inputs from individual RA- and SA- touch sensory neurons extensively diverge into multiple sub-locations within a vibrissa column. There is no stereotypic spatial organization of RA- versus SA- collaterals at the single-neuron level, consistent with the intermixed projections patterns observed in the population analysis.

Convergent RA and SA inputs onto second-order projection neurons

The above genetic tracing experiments suggest that there are *unlikely* anatomically segregated labeled-lines (or sub-columns) for RA- and SA- afferents within the individual vibrissa column. However, the second-order thalamic-projecting neurons could in principle receive *selective* inputs from only RA- or SA- afferents. In other words, there might be "hidden" labeled-lines at the connectivity level without apparent spatial segregation. To address this question, we devised a 4-color strategy to simultaneously label (1) RA-lanceolate-axons (Chodl^{PLAP} labeled), (2) SA-Merkel-axons (Pv::Cre; RΦtomato labeled axons not overlapping with Chodl^{PLAP}), (3) presynaptic sites (vGluT1 staining), and (4) brainstem projection neurons (retrogradely labeled from thalamus). It is known that PrV projection neurons (PNs) primarily send axons to the ventral posterior medial (VPM) nucleus of the thalamus, whereas SpI PNs mainly project to the posterior medial nucleus (PoM) of the thalamus. We used the deficient rabies virus expressing GFP (ΔG-RV-GFP) injected into either VPM or PoM to retrogradely label PrV-PNs or SpI-PNs (Wickersham et al., 2007) (fig. S5A). Many morphologically different types of PNs were labeled throughout all four brainstem nuclei using the retrograde virus (examples are shown in fig. S5B). Since examining RA and SA afferent inputs onto all types of PNs was beyond the scope of this study, we only examined PNs located in the barrelette regions in SpI and in PrV, with primary focus on those that had dendrites restricted to individual barrelettes (i.e. barrelette cells) (e.g. Fig. 4B1, right PN in Fig. 4B2, and Fig. 4D1), though we also examined a few multi-barrelettes cells (left PN in Fig. 4B2, and Fig. 4D2).

Representative results from such 4-color experiments with sparsely labeled PNs in SpI and PrV (age P7) are shown (Fig. 4A, 4C). As expected for this stage (P7), Pv-tomato only labeled a subset of SA-Merkel neurons in large barrelettes. Chodl^{PLAP}/vGluT1/GFP triple-

positive spots on each of the z-stacks were extracted out as synapses formed between the RA-lanceolate afferents and the PNs, and depicted as green dots on the grey PNs (Fig. 4B, 4D, right-most panel). Pv-tomato/vGluT1/GFP triple-positive spots that did *not* overlap with $Chodl^{PLAP}$ were extracted out as synapses formed between the SA-Merkel afferents and the PNs, and depicted as red dots on the grey PNs (Fig. 4B, 4D, right-most panels). All PNs (n=50) in both SpI and PrV examined by this method (including both barrelette cells and multi-barrelettes cells) had both RA and SA synapses on them (Fig. 4, additional representative examples shown in fig. S6, and data not shown). In many PNs (especially in PrV), it is difficult to distinguish whether the distal dendrites belong to the same neuron or neighboring neurons. In these cases, we examined only the cell bodies and the proximal dendrites of the PNs, and still observed that all PNs received both RA and SA inputs (Fig. 4B, 4D and fig. S6). Because Pv-tomato only partially labeled the SA-Merkel afferents at this stage, we could not quantify the relative amounts of RA- versus SA- synapses onto a PN. But suffice it to say, convergence of RA and SA synapses onto individual second-order PNs is a general theme in the organization of vibrissa sensory circuits.

DISCUSSION

Using a combination of genetic and viral techniques to specifically label different types of touch sensory afferents and second-order projection neurons (PNs) with different colors, we dissected the connectivity of the mouse vibrissae touch sensory circuit. At the population level, axonal projections and synapses formed by neurons of two submodalities (RA-lanceolate and SA- Merkel neurons) are spatially intermingled and variably distributed, with no reproducible patterns among different vibrissa barrelettes or across different animals. At the single neuron level, consistent with previous HRP-based axon-tracing experiments (Hayashi, 1985; Jacquin et al., 1993; Jacquin et al., 1988; Jacquin et al., 1986), a single lanceolate- or Merkel-ending neuron projects multiple collaterals within one barrelette, thus likely forming synapses with multiple PNs. Individual PNs receive convergent afferent inputs from both RA- and SA- submodalities. Taken together, our findings support a “one-to-many and many-to-one” connectivity scheme, with substantial divergence and convergence of afferents onto PNs and *no* ordered labeled-line-like segregation of RA- and SA-specific inputs inside individual vibrissa columns (see model in Fig.5).

Although with the exception of longitudinal lanceolate- (RA) and Merkel-endings (SA) neurons, the adaptation properties of other types of touch neurons are unknown, the observed convergence of RA-lanceolate and SA-Merkel afferents onto second-order PNs already predicts that PNs will exhibit *mixed* RA and SA responses. In other words, PNs should show both phasic ON/OFF responses and intermediate tonic responses toward a “ramp-and-hold” stimulus (illustrated in Fig. 5A). Given the uneven patchy distributions of RA- and SA- synapses, it is conceivable that some PNs may receive more RA- or SA- inputs and are therefore be more RA-like or SA-like; while many others may receive equivalent RA- and SA- inputs and therefore show mixed responses. This prediction is in complete agreement with previous in vivo electrophysiology recordings of brainstem PNs (Minnery and Simons, 2003). In those studies, Minnery and Simon found that strict tonic (SA) or phasic (RA) PNs did *not* exist, rather a continuum of PN responses was observed: all PN neurons displayed different degrees of sustained firing during the “hold” portion of the stimulus (Minnery and Simons, 2003).

In the dorsal root ganglia (DRG) system, a recent work on mechanosensory neurons innervating hairy skin revealed that 3 different types of RA-lanceolate ending neurons segregated their central axons into 3 different layers in the spinal cord dorsal horn (Li et al., 2011). In that case, the 3 types of lanceolate neurons are of three different fiber types: Aβ (heavily-myelinated), Aδ (thinly-myelinated), and c-fibers (unmyelinated) (Li et al., 2011);

whereas our study here examined trigeminal touch neurons within the Aβ category. In fact, in the DRG system, it is also known that the Aβ class of RA- and SA- DRG afferents both project to spinal layers III–V, and there had been no studies suggesting any kind of spatial segregation (Woodbury and Koerber, 2007; Woodbury et al., 2001). Of course, our 4-color labeling studies were difficult experiments and thus have their technical limitations. In addition, we have not yet examined all types of PNs, therefore we could not rule out the possibility that certain type of PNs might receive predominantly one sub-modality type of inputs. However, given that all PNs we examined received both RA and SA inputs, and taken together with previous in vivo recordings results (Bellavance et al., 2010; Minnery and Simons, 2003), we are confident that convergence of sub-modality-specific inputs onto PNs is a general theme in the touch sensory system.

Notably, the original idea that RA and SA inputs are segregated into labeled-lines came from previous studies in primates (monkeys), in which the large cortical column representing a digit was found to divide into RA and SA sub-columns (Sur et al., 1984). However, recent recordings studies revisited this issue, and it was found that a major proportion of neurons in the monkey somatosensory cortex actually receive convergent RA and SA inputs, i.e. they exhibited mixed ON/OFF and sustained responses (Pei et al., 2009). Other imaging studies also support the lack of separate processing streams for RA and SA sub-modalities in the somatosensory cortex in primates (Chen et al., 2001; Friedman et al., 2004).

What are the implications of this “one-to-many and many-to-one” connectivity scheme inside a single vibrissa column for touch information encoding and processing? It is known that rats and mice could perform tactile discrimination tasks with just a single vibrissa (e.g (Hutson and Masterton, 1986)). Here we propose a hypothetical model involving temporal coding that could explain the discriminatory ability of a single vibrissa (Fig. 5B). We hypothesize that upon touching a natural object, a subset of touch sensory neurons inside the vibrissa (of both RA and SA types) are activated. Based on previous electrophysiology studies (such as (Szwed et al., 2003)), activated neurons are likely to fire with slightly different timing of onset, resulting in differences in spike-timing and first-spike latency across the population (Fig. 5B left panel). We *speculate* that the second-order PNs function as coincidence detectors, i.e. they prefer to fire when they receive synchronous inputs. With the “one-to-many and many-to-one” unstructured connectivity, the “transient synchrony” of a few afferent spikes will arrive at different second-order PNs with different timing (Fig. 5B right panel). In this manner, different touch stimuli trigger distinct spatiotemporal firing sequences of PNs receiving inputs from that vibrissa, resulting in distinct temporal codes. Thus, with the use of temporal codes (which is unlimited), even a single vibrissa could encode and discriminate diverse textures and forms. Future electrophysiological studies of brainstem PNs, such as those that examine the spike-triggered stimulus average and spike-triggered stimulus correlation across populations of PNs, will test our model and inform us whether these neurons indeed function as coincidence detectors and what is their physiological time window of integration (Stéphanie et al., 2013). On a broader perspective, it is interesting to note that spike-timing of peripheral afferents with millisecond precision was also shown to play important roles in encoding and decoding tactile information in monkeys (Mackevicius et al., 2012). Our model invoking both the spike-timing difference of touch receptor firing and detection of synchronous spikes by PNs is similar to what has been proposed for how tactile information is encoded by the fingertip sensory neurons and their associated circuits in humans (Johansson and Flanagan, 2009).

EXPERIMENTAL PROCEDURES

Mouse

Chodl^{PLAP} mutant mice: An hPLAP-ACN cassette (Zylka et al., 2005) was inserted into the translation start ATG of the *Chondrolectin* gene to generate Chodl^{PLAP} mice. Pv::CreERt2 mice: A CreERt2 was inserted into Pv locus to generate Pv::CreERt2 mice using a strategy analogous to the one described previously (Hippenmeyer et al., 2005). Pv::Cre mice (stock#008069) was purchased from the Jackson Laboratories. RΦAP, RΦGFP and RΦtomato mice were all generated in our laboratory (Arenkiel et al., 2011; da Silva et al., 2011; Que et al., 2008).

All experiments were conducted according to protocols approved by The Duke University Institutional Animal Care and Use Committee.

Tamoxifen Injections

The tamoxifen solution (0.05–0.1mg/g (Body Weight)) was injected subcutaneously into the back to Pv::CreERt2; RΦtomato mice at P1 (for P8 sample collection) or at P5 (for P28 sample collection).

Deficient rabies virus retrograde tracing experiment

Pv::Cre; RΦtomato; Chodl$^{PLAP/+}$ mice were anesthetized with ketamine/xylazine (50 mg/kg, 5 mg/kg, respectively, i.p.) at P4 and injected with ΔG-GFP-RV into right side of the VPM and PoM regions of thalamus. Brains were collected 3 days post infection.

Histological analysis

Immunostaining, alkaline phosphatase staining and in situ hybridization were performed according to standard procedures. For PLAP immunostaining, tissue sections were incubated in 10mM sodium citrate buffer (pH8.5) at 80°C for 30 min before blocking. For 4-color immunostaining (GFP, PLAP, vGluT1 and tomato), tissue sections were incubated with Image-iT Signal Enhancer (Invitrogen) at room temperature for 1h after antigen retrieval. The primary antibodies used for this study were: rabbit anti-RFP (Rockland, 600401379, 1:1000), chicken anti-GFP (Invitrogen, A10262, 1:1000), guinea-pig anti-vGlut1 (Millipore, AB5905, 1:1000), mouse anti-PLAP (Sigma, A2951, 1:1000), rat anti-CK8 (anti-Troma1) (Univ of Iowa/DSHB, 1:1000), rabbit anti-NF200 (Sigma, 1:1000).

Preparation of confocal stacks for image processing

Z-stack images were taken by Zeiss 710 to cover the entire thickness of the sections. A z-stack image was imported into ImageJ-based FIji software and transformed into a multi-color *tiff* format file. This z-stack *tiff* images were used for subsequent image processing.

Generating synapse maps for lanceolate- and Merkel-ending neurons

To map the locations of presynaptic termini for longitudinal lanceolate- or Merkel-ending neurons within the each barrelette for each z-stack series, we processed images using Fiji and Imaris software (Bitplane). By using “Coloc plugin” of Imaris software, first, vGluT1 and Chodl^{PLAP} double positive sites, which represented lanceolate-ending presynaptic termini, were extracted from all z-stack images. Similarly, vGluT1 and tomato co-labeled sites, which represented Merkel and a subset of lanceolate-ending synapses, were extracted from all z-stack images. To visualize Merkel-ending-only synapses, Chodl^{PLAP}, vGluT1, and tomato triple-positive spots were removed from the vGluT1 and tomato double-positive sites by using “Mask” function. The extracted synapses were reconstructed in 3D by using the “Surface” function of Imaris.

Generating 2D-projected heatmaps for RA-lanceolate and SA-Merkel synapses

The extracted z-stack images of RA-lanceolate or SA-Merkel synapses were combined into one large z-stack image using Fiji. Each single optical image of the z-stack is divided into 550×550 (x,y) pixels. The pixel either contains synapses (pixel value=1) or does not contain any synapse (pixel value=0). The total number of pixels in the combined z-stack is thus 550×550×N (N=the total number of single optical images). In order to obtain 2D heatmaps of synaptic densities for each type of afferents, the pixels (and their values) are projected onto three 2D planes: coronal (x, y); lateral/sagittal (y, z), and horizontal (x, z), as illustrated in supplemental figure S4A. The values of the projected pixels are represented as heatmaps by using *colormap* function in MATLAB. The color represents relative synaptic densities in each sample.

3D reconstruction and image analysis of single-labeled neuron

The cropping, alignment and converting into one z-stack image were performed using the same procedure as described in “generating synapse maps for lanceolate and Merkel-ending neurons”. The volume of barrelette of each section was calculated as follows; “Area” × “Number of z-stack images” × “Voxel depth”. The 3D reconstructed images were made by Fiji or Imaris software. The Imaris software allowed us to calculate the number of voxels (three-dimensional pixel) that the axon or the presynaptic termini occupy on the 3D dataset reconstructed from z-stacks. The normalized collateral volumes were calculated as follows; “Number of voxels of axon collaterals” × “Volume of one voxel” / “Volume of the barrelette”. The synaptic densities were calculated as follows; “Number of voxels of presynaptic termini” / “Number of voxels of axon collaterals”.

Analyzing presynaptic termini onto retrogradely labeled projection neurons (PNs)

A z-stack image was imported into Imaris software. Chodl^{PLAP}/vGluT1/GFP (GFP labels PNs) triple-positive spots (RA-lanceolate presynaptic loci onto PNs) and Pv-tomato/vGluT1/GFP triple-positive spots (SA-Merkel and a subset of RA-lanceolate presynaptic loci onto PN) were detected by using Spot Detection function of Imaris, and plotted onto the PNs. Chodl^{PLAP}/tomato/vGluT1/GFP quadruple-positive spots were considered as RA-lanceolate synaptic loci.

Statistical analysis

Student’s t-test was used where appropriate. Results are displayed as mean ± SEM.

For full details of methods, please refer to Extended Experimental Procedures.

Supplementary Material

Refer to Web version on PubMed Central for supplementary material.

Acknowledgments

We thank Duke Cancer Center transgenic facility for blastocyst injections that generated Chodl$^{PLAP/+}$ mice. We thank Dr. Kosuke Hamaguchi for help with custom written programs in MATLAB. We thank Duke Light Microscopy Core facility for help with confocal imaging and 3D reconstruction. This work is supported by NIH RO1 DE019440 and NS077986 to F.W., and Swiss National Foundation, Kanton Basel-Stadt, ERC Advanced Grant and Novartis Research Foundation to S.A.

REFERENCES

Arber S, Ladle DR, Lin JH, Frank E, Jessell TM. ETS gene Er81 controls the formation of functional connections between group Ia sensory afferents and motor neurons. Cell. 2000; 101:485–498. [PubMed: 10850491]

Arenkiel BR, Hasegawa H, Yi JJ, Larsen RS, Wallace ML, Philpot BD, Wang F, Ehlers MD. Activity-induced remodeling of olfactory bulb microcircuits revealed by monosynaptic tracing. PloS one. 2011; 6:e29423. [PubMed: 22216277]

Bellavance MA, Demers M, Deschenes M. Feedforward inhibition determines the angular tuning of vibrissal responses in the principal trigeminal nucleus. The Journal of neuroscience : the official journal of the Society for Neuroscience. 2010; 30:1057–1063. [PubMed: 20089914]

Bennett-Clarke CA, Chiaia NL, Jacquin MF, Rhoades RW. Parvalbumin and calbindin immunocytochemistry reveal functionally distinct cell groups and vibrissa-related patterns in the trigeminal brainstem complex of the adult rat. The Journal of comparative neurology. 1992; 320:323–338. [PubMed: 1377200]

Bosman LW, Houweling AR, Owens CB, Tanke N, Shevchouk OT, Rahmati N, Teunissen WH, Ju C, Gong W, Koekkoek SK, De Zeeuw CI. Anatomical pathways involved in generating and sensing rhythmic whisker movements. Frontiers in integrative neuroscience. 2011; 5:53. [PubMed: 22065951]

Carvell GE, Simons DJ. Biometric analyses of vibrissal tactile discrimination in the rat. The Journal of neuroscience : the official journal of the Society for Neuroscience. 1990; 10:2638–2648. [PubMed: 2388081]

Chen LM, Friedman RM, Ramsden BM, LaMotte RH, Roe AW. Fine-scale organization of SI (area 3b) in the squirrel monkey revealed with intrinsic optical imaging. Journal of neurophysiology. 2001; 86:3011–3029. [PubMed: 11731557]

da Silva S, Hasegawa H, Scott A, Zhou X, Wagner AK, Han BX, Wang F. Proper formation of whisker barrelettes requires periphery-derived Smad4-dependent TGF-beta signaling. Proceedings of the National Academy of Sciences of the United States of America. 2011; 108:3395–3400. [PubMed: 21300867]

Ebara S, Kumamoto K, Matsuura T, Mazurkiewicz JE, Rice FL. Similarities and differences in the innervation of mystacial vibrissal follicle-sinus complexes in the rat and cat: a confocal microscopic study. The Journal of comparative neurology. 2002; 449:103–119. [PubMed: 12115682]

Enjin A, Rabe N, Nakanishi ST, Vallstedt A, Gezelius H, Memic F, Lind M, Hjalt T, Tourtellotte WG, Bruder C, et al. Identification of novel spinal cholinergic genetic subtypes disclose Chodl and Pitx2 as markers for fast motor neurons and partition cells. The Journal of comparative neurology. 2010; 518:2284–2304. [PubMed: 20437528]

Ernfors P, Lee KF, Kucera J, Jaenisch R. Lack of neurotrophin-3 leads to deficiencies in the peripheral nervous system and loss of limb proprioceptive afferents. Cell. 1994; 77:503–512. [PubMed: 7514502]

Erzurumlu RS, Murakami Y, Rijli FM. Mapping the face in the somatosensory brainstem. Nature reviews. Neuroscience. 2010; 11:252–263.

Friedman RM, Chen LM, Roe AW. Modality maps within primate somatosensory cortex. Proceedings of the National Academy of Sciences of the United States of America. 2004; 101:12724–12729. [PubMed: 15308779]

Gottschaldt KM, Iggo A, Young DW. Functional characteristics of mechanoreceptors in sinus hair follicles of the cat. The Journal of physiology. 1973; 235:287–315. [PubMed: 4763992]

Hasegawa H, Abbott S, Han BX, Qi Y, Wang F. Analyzing somatosensory axon projections with the sensory neuron-specific Advillin gene. The Journal of neuroscience : the official journal of the Society for Neuroscience. 2007; 27:14404–14414. [PubMed: 18160648]

Hasegawa H, Wang F. Visualizing mechanosensory endings of TrkC-expressing neurons in HS3ST-2-hPLAP mice. The Journal of comparative neurology. 2008; 511:543–556. [PubMed: 18839409]

Hayashi H. Morphology of central terminations of intra-axonally stained, large, myelinated primary afferent fibers from facial skin in the rat. The Journal of comparative neurology. 1985; 237:195–215. [PubMed: 2993374]

Hippenmeyer S, Vrieseling E, Sigrist M, Portmann T, Laengle C, Ladle DR, Arber S. A developmental switch in the response of DRG neurons to ETS transcription factor signaling. PLoS biology. 2005; 3:e159. [PubMed: 15836427]

Hutson KA, Masterton RB. The sensory contribution of a single vibrissa's cortical barrel. Journal of neurophysiology. 1986; 56:1196–1223. [PubMed: 3783236]

Ichikawa H, Sugimoto T. Calcium-binding protein-immunoreactive innervation of the rat vibrissa. Brain research. 2003; 970:226–231. [PubMed: 12706265]

Jacquin MF, Renehan WE, Rhoades RW, Panneton WM. Morphology and topography of identified primary afferents in trigeminal subnuclei principalis and oralis. Journal of neurophysiology. 1993; 70:1911–1936. [PubMed: 8294963]

Jacquin MF, Stennett RA, Renehan WE, Rhoades RW. Structure-function relationships in the rat brainstem subnucleus interpolaris: II. Low and high threshold trigeminal primary afferents. The Journal of comparative neurology. 1988; 267:107–130. [PubMed: 3343389]

Jacquin MF, Woerner D, Szczepanik AM, Riecker V, Mooney RD, Rhoades RW. Structure-function relationships in rat brainstem subnucleus interpolaris. I. Vibrissa primary afferents. The Journal of comparative neurology. 1986; 243:266–279. [PubMed: 3944280]

Johansson RS, Flanagan JR. Coding and use of tactile signals from the fingertips in object manipulation tasks. Nature reviews. Neuroscience. 2009; 10:345–359.

Killackey HP, Rhoades RW, Bennett-Clarke CA. The formation of a cortical somatotopic map. Trends in neurosciences. 1995; 18:402–407. [PubMed: 7482806]

Li L, Rutlin M, Abraira VE, Cassidy C, Kus L, Gong S, Jankowski MP, Luo W, Heintz N, Koerber HR, et al. The functional organization of cutaneous low-threshold mechanosensory neurons. Cell. 2011; 147:1615–1627. [PubMed: 22196735]

Lichtenstein SH, Carvell GE, Simons DJ. Responses of rat trigeminal ganglion neurons to movements of vibrissae in different directions. Somatosensory & motor research. 1990; 7:47–65. [PubMed: 2330787]

Lumpkin EA, Marshall KL, Nelson AM. The cell biology of touch. The Journal of cell biology. 2010; 191:237–248. [PubMed: 20956378]

Luo W, Enomoto H, Rice FL, Milbrandt J, Ginty DD. Molecular identification of rapidly adapting mechanoreceptors and their developmental dependence on ret signaling. Neuron. 2009; 64:841–856. [PubMed: 20064391]

Mackevicius EL, Best MD, Saal HP, Bensmaia SJ. Millisecond precision spike timing shapes tactile perception. The Journal of neuroscience : the official journal of the Society for Neuroscience. 2012; 32:15309–15317. [PubMed: 23115169]

Minnery BS, Simons DJ. Response properties of whisker-associated trigeminothalamic neurons in rat nucleus principalis. Journal of neurophysiology. 2003; 89:40–56. [PubMed: 12522158]

Pei YC, Denchev PV, Hsiao SS, Craig JC, Bensmaia SJ. Convergence of submodality-specific input onto neurons in primary somatosensory cortex. Journal of neurophysiology. 2009; 102:1843–1853. [PubMed: 19535484]

Que J, Wilm B, Hasegawa H, Wang F, Bader D, Hogan BL. Mesothelium contributes to vascular smooth muscle and mesenchyme during lung development. Proceedings of the National Academy of Sciences of the United States of America. 2008; 105:16626–16630. [PubMed: 18922767]

Rice FL, Fundin BT, Arvidsson J, Aldskogius H, Johansson O. Comprehensive immunofluorescence and lectin binding analysis of vibrissal follicle sinus complex innervation in the mystacial pad of the rat. The Journal of comparative neurology. 1997; 385:149–184. [PubMed: 9268122]

Rice FL, Mance A, Munger BL. A comparative light microscopic analysis of the sensory innervation of the mystacial pad. I. Innervation of vibrissal follicle-sinus complexes. The Journal of comparative neurology. 1986; 252:154–174. [PubMed: 3782505]

Stéphanie R, Sungho H, Erik DS, Prescott SA. Impact of Neuronal Properties on Network Coding: Roles of Spike Initiation Dynamics and Robust Synchrony Transfer. Neuron. 2013; 78:758–772. [PubMed: 23764282]

Sur M, Wall JT, Kaas JH. Modular distribution of neurons with slowly adapting and rapidly adapting responses in area 3b of somatosensory cortex in monkeys. Journal of neurophysiology. 1984; 51:724–744. [PubMed: 6716121]

Szwed M, Bagdasarian K, Ahissar E. Encoding of vibrissal active touch. Neuron. 2003; 40:621–630. [PubMed: 14642284]

Welker E, Van der Loos H. Quantitative correlation between barrel-field size and the sensory innervation of the whiskerpad: a comparative study in six strains of mice bred for different patterns of mystacial vibrissae. The Journal of neuroscience : the official journal of the Society for Neuroscience. 1986; 6:3355–3373. [PubMed: 3772437]

Weng L, Hubner R, Claessens A, Smits P, Wauters J, Tylzanowski P, Van Marck E, Merregaert J. Isolation and characterization of chondrolectin (Chodl), a novel C-type lectin predominantly expressed in muscle cells. Gene. 2003; 308:21–29. [PubMed: 12711387]

Wickersham IR, Finke S, Conzelmann KK, Callaway EM. Retrograde neuronal tracing with a deletion-mutant rabies virus. Nature methods. 2007; 4:47–49. [PubMed: 17179932]

Woodbury CJ, Koerber HR. Central and peripheral anatomy of slowly adapting type I low-threshold mechanoreceptors innervating trunk skin of neonatal mice. The Journal of comparative neurology. 2007; 505:547–561. [PubMed: 17924532]

Woodbury CJ, Ritter AM, Koerber HR. Central anatomy of individual rapidly adapting low-threshold mechanoreceptors innervating the "hairy" skin of newborn mice: early maturation of hair follicle afferents. The Journal of comparative neurology. 2001; 436:304–323. [PubMed: 11438932]

Woolsey TA, Van der Loos H. The structural organization of layer IV in the somatosensory region (SI) of mouse cerebral cortex. The description of a cortical field composed of discrete cytoarchitectonic units. Brain research. 1970; 17:205–242. [PubMed: 4904874]

Zylka MJ, Rice FL, Anderson DJ. Topographically distinct epidermal nociceptive circuits revealed by axonal tracers targeted to Mrgprd. Neuron. 2005; 45:17–25. [PubMed: 15629699]

Highlights

1. The connectivity of submodality-specific touch afferent circuit is visualized.
2. Inputs from SA and RA touch afferents are spatially intermixed with no stereotypy.
3. Single touch neuron projects collaterals to multiple locations within a column.
4. Second-order projection neurons receive convergent inputs from RA and SA afferents.

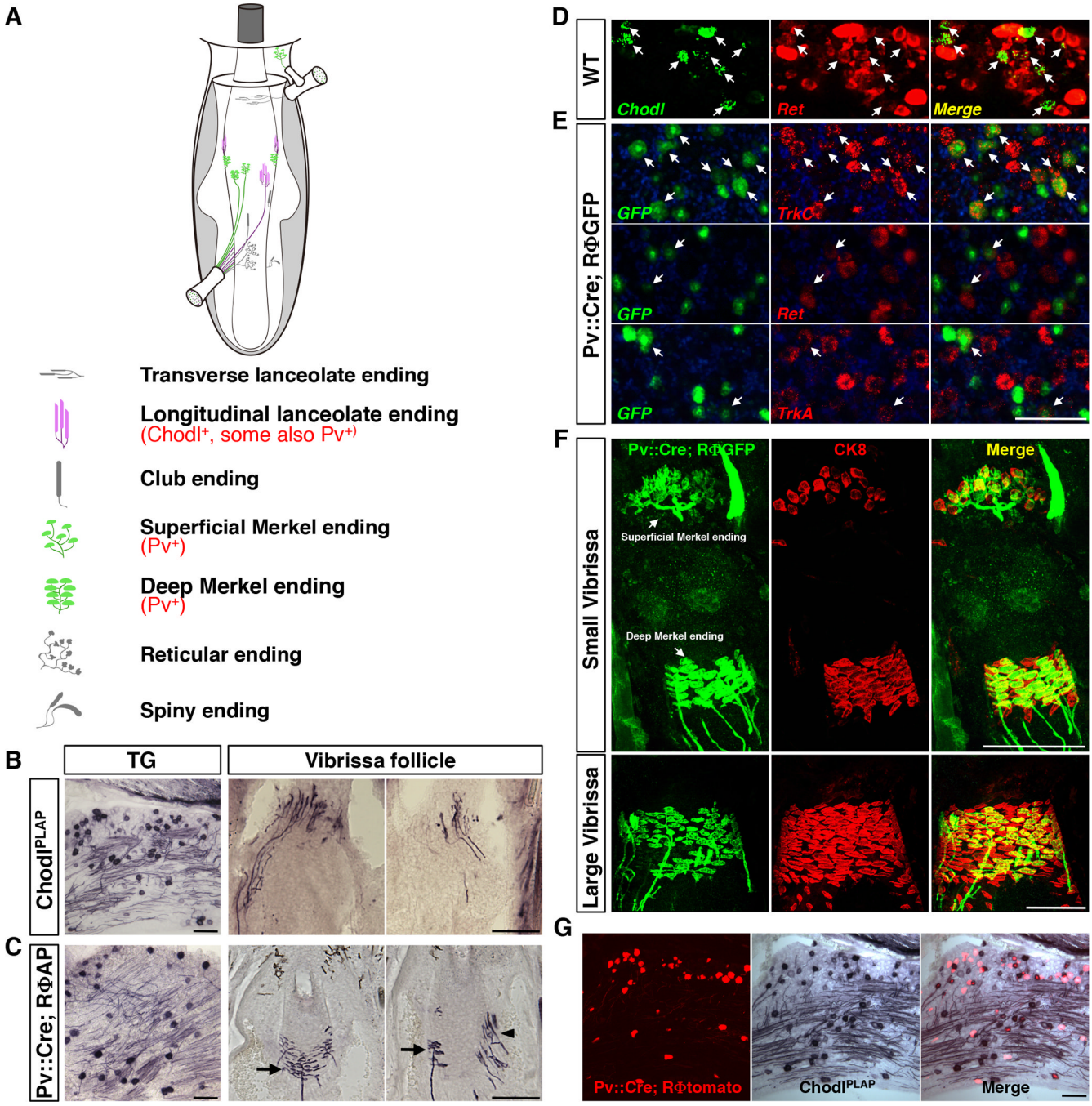

Fig. 1. Genetic labeling of RA-longitudinal lanceolate and SA-Merkel ending neurons in the vibrissa sensory system

(**A**) Schematic drawing of the types of touch sensory endings in the mouse vibrissa follicle.

(**B**) Representative images of AP staining result from P7 Chodl$^{PLAP/+}$ mice on trigeminal ganglion (TG) section (left) and vibrissa follicle sections (right two panels). Longitudinal-lanceolate-ending neurons were selectively labeled.

(**C**) Representative images of AP staining result from P7 Pv::Cre; RΦAP mice on TG (left) or vibrissa follicle sections (right two panels). Pv::Cre; RΦAP labeled Merkel-ending (arrow) and a few longitudinal lanceolate-ending (arrowhead) neurons.

(**D**) Representative images of 2-color fluorescent in situ hybridization with C*hodl* (green) and *Ret* (red) probes on the P7 WT TG sections. 96.46 ± 0.27% *chodl*+ cells co-expressed Ret (arrow).
(**E**) Representative images of 2-color fluorescent in situ hybridization on TG sections from P21 Pv::Cre; RΦGFP mice. Top row: *GFP* (green) and *TrkC* (red); middle row: *GFP* and *Ret*; bottom row: *GFP* and TrkA. 62.4 ± 1.5% *GFP*+ cells (labeled by Pv::Cre) co-expressed with *TrkC*. 25.6 ± 1.0% *GFP*+ cells co-expressed with *Ret*. 17.3 ± 2.9% *GFP*+ cells co-expressed with *TrkA*.
(**F**) Double immunostaining showing sensory axons (green) and Merkel cells (red) on sections from the mystacial pad from Pv::Cre; RΦGFP mice at P7. In the small vibrissa (top row), more than 90% of Merkel cells were innervated by Pv::Cre labeled axons; in contrast, in the large vibrissa (bottom row images), Pv::Cre only labeled subsets of axons innervating Merkel cells.
(**G**) Representative TG sections from Pv::Cre; RΦtomato; Chodl$^{PLAP/+}$ triple transgenic mice (P7). 22.3 ± 0.8% Chodl+ (AP stained) neurons exhibit tomato fluorescence (PLAP and tomato double positive). Conversely, 24.3 ± 1.3% tomato+ neurons exhibit PLAP activity (Chodl+).
Scale bars: 100 μm.
See also Figure S1.

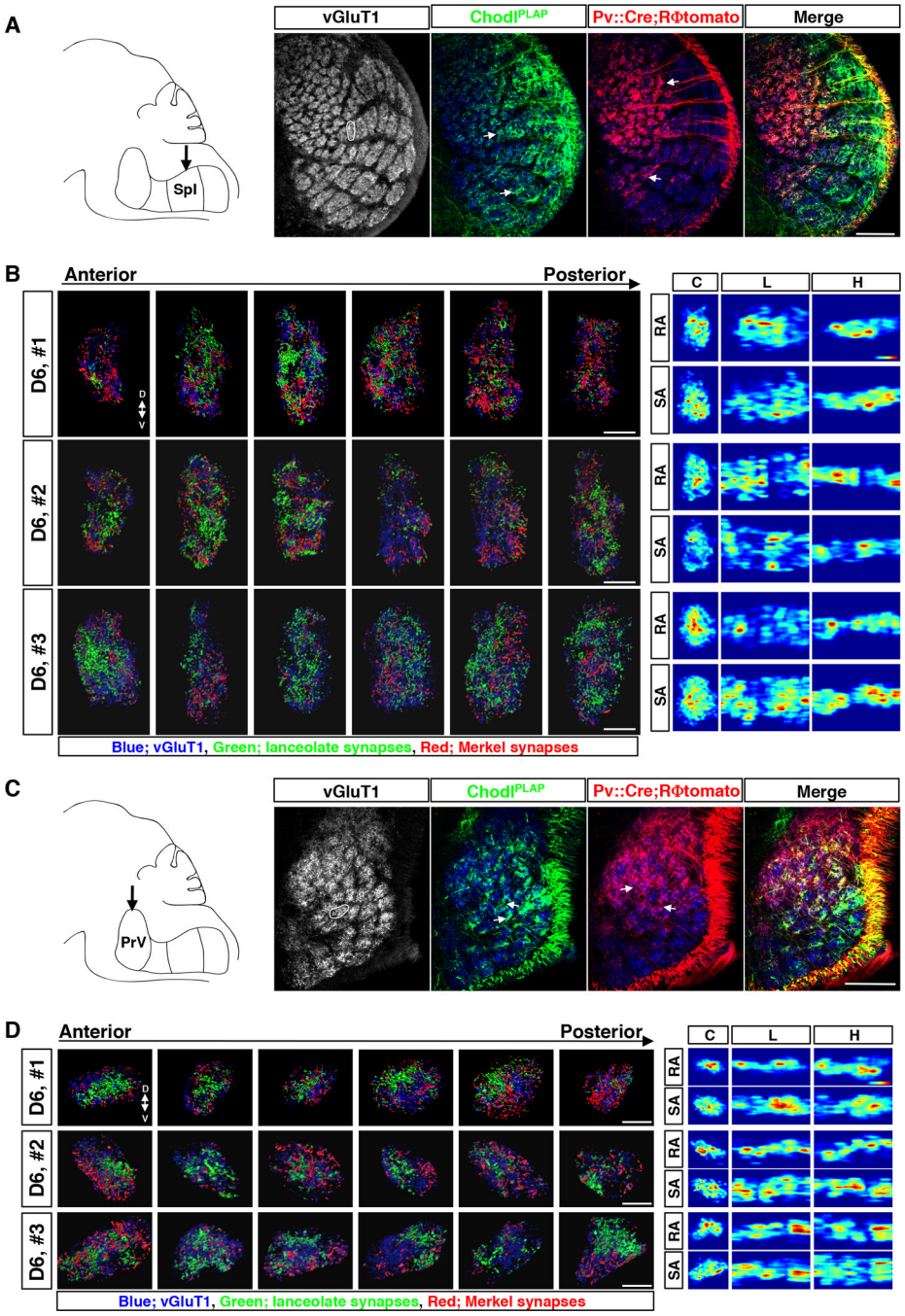

Fig. 2. Axonal projections and presynaptic termini distribution maps of RA-longitudinal lanceolate and SA-Merkel ending neurons within individual barrelette columns in SpI and PrV nuclei

(**A, C**) Left panel: Schematic drawing of the brainstem trigeminal complex (sagittal view) with arrow indicating the SpI (A) or PrV (C) nucleus. Right 4 panels: Representative images of immunostaining of vGluT1 (grey or blue), PLAP (green) and tomato (red) on the sections of SpI (**A**) or PrV (**C**) nucleus from Pv::Cre; RΦtomato; Chodl^{PLAP} mice (P7). White circle indicates the D6 barrelette. White arrows indicate examples of dense patches of afferent termini. All images are of coronal view.

(**B, D**) Maps of afferent presynaptic termini inside D6 barrelette in SpI (**B**) or PrV (**D**) nucleus from 3 different samples (numbered 1–3). Left panels show representative results of presynaptic sites extracted from confocal images of individual serial sections through each D6 barrelette in Spl (B) or PrV (D). Blue: vGluT1+ loci. Green: presynaptic termini of RA afferents (PLAP+ ∩ vGluT1+). Red: presynaptic termini of SA afferents ((tomato+ ∩ vGluT1+) − (PLAP+ ∩ vGluT1+)). Right panels show the heatmaps of RA- and SA-synaptic densities in each sample; 2D projections of the 3D data from each barrelette column onto 3 different planes are shown. C, coronal plane; L, lateral/sagittal plane; H, horizontal plane. The color on heatmaps represents *relative* synaptic density in each sample. The highest density is shown as red. The lowest density is shown as blue.
Scale bars: 100 μm (A, C), 20 μm (B, D).
See also Figure. S1, S2, S3 and Movie S1, S2.

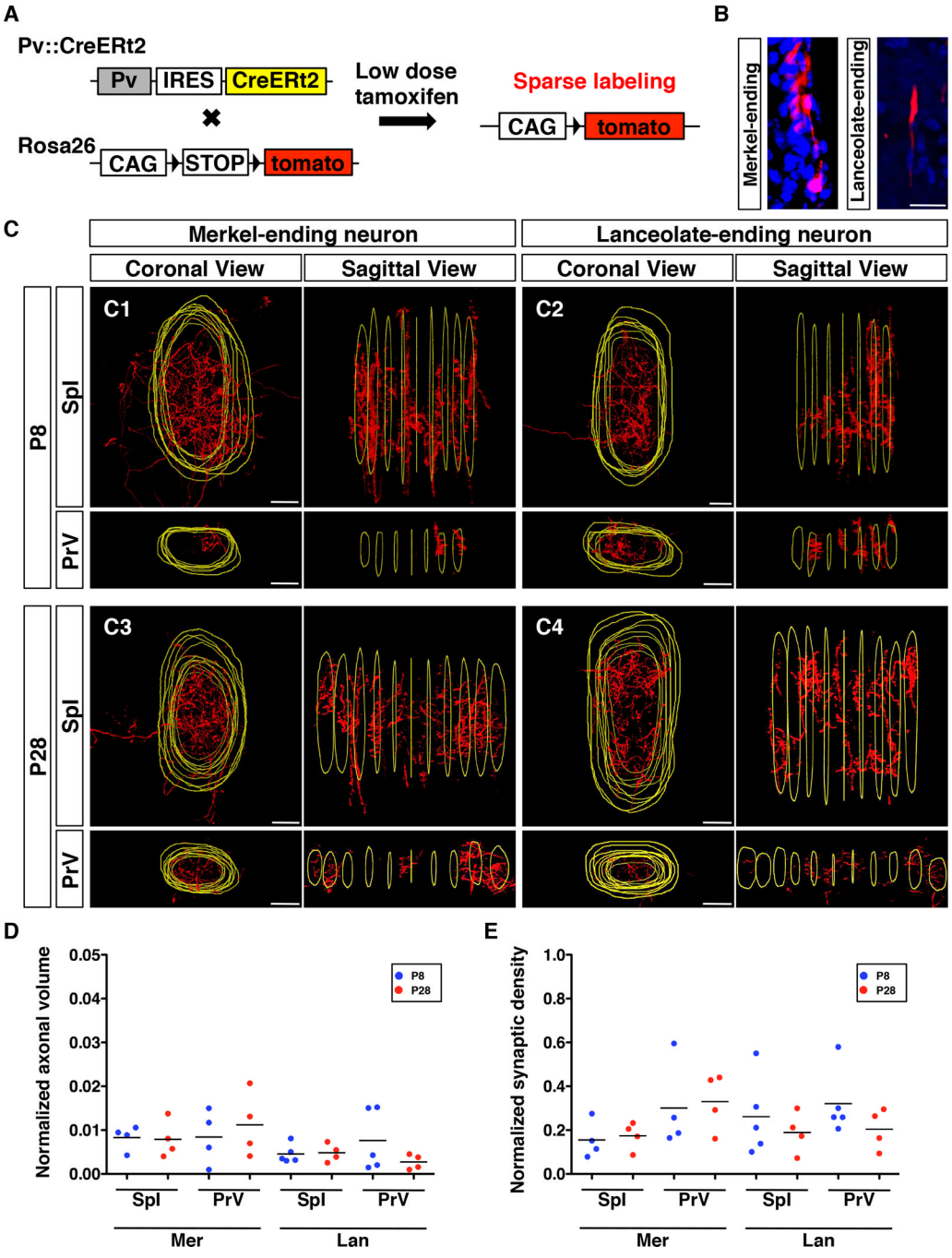

Fig. 3. Axon collaterals of single-labeled RA-lanceolate and SA-Merkel neurons inside the barrelette unit

(**A**) Schematic representation of the strategy used to sparsely label longitudinal lanceolate and Merkel-ending neurons.

(**B**) Representative images of the peripheral ending of single-labeled Merkel or lanceolate neuron. Red, axon; Blue, DAPI.

(**C**) Representative coronal views and lateral/sagittal views of 3D reconstructed collaterals from single-labeled Merkel and single-labeled lanceolate neuron in the SpI and PrV at P8 and P28, respectively. Red, axon; Yellow, outlines of the barrelette structure.

(**D**) Quantification of relative volumes occupied by axon collaterals of single-labeled Merkel or lanceolate neurons normalized with respect to the volume of each corresponding barrelette column. All comparisons between P8 and P28 are not statistically different ($p>0.05$, t-test).
(**E**) Quantification of relative synaptic densities of single-labeled Merkel or lanceolate neurons normalized with respect to the total volume of the collaterals. All comparisons between P8 and P28 are not statistically different ($p>0.05$, t-test).
Abbreviations: Mer, Merkel-ending neuron; Lan, lanceolate-ending neuron. Scale bars: 20 μm.
See also Figure S4 and Movie S3–S6.

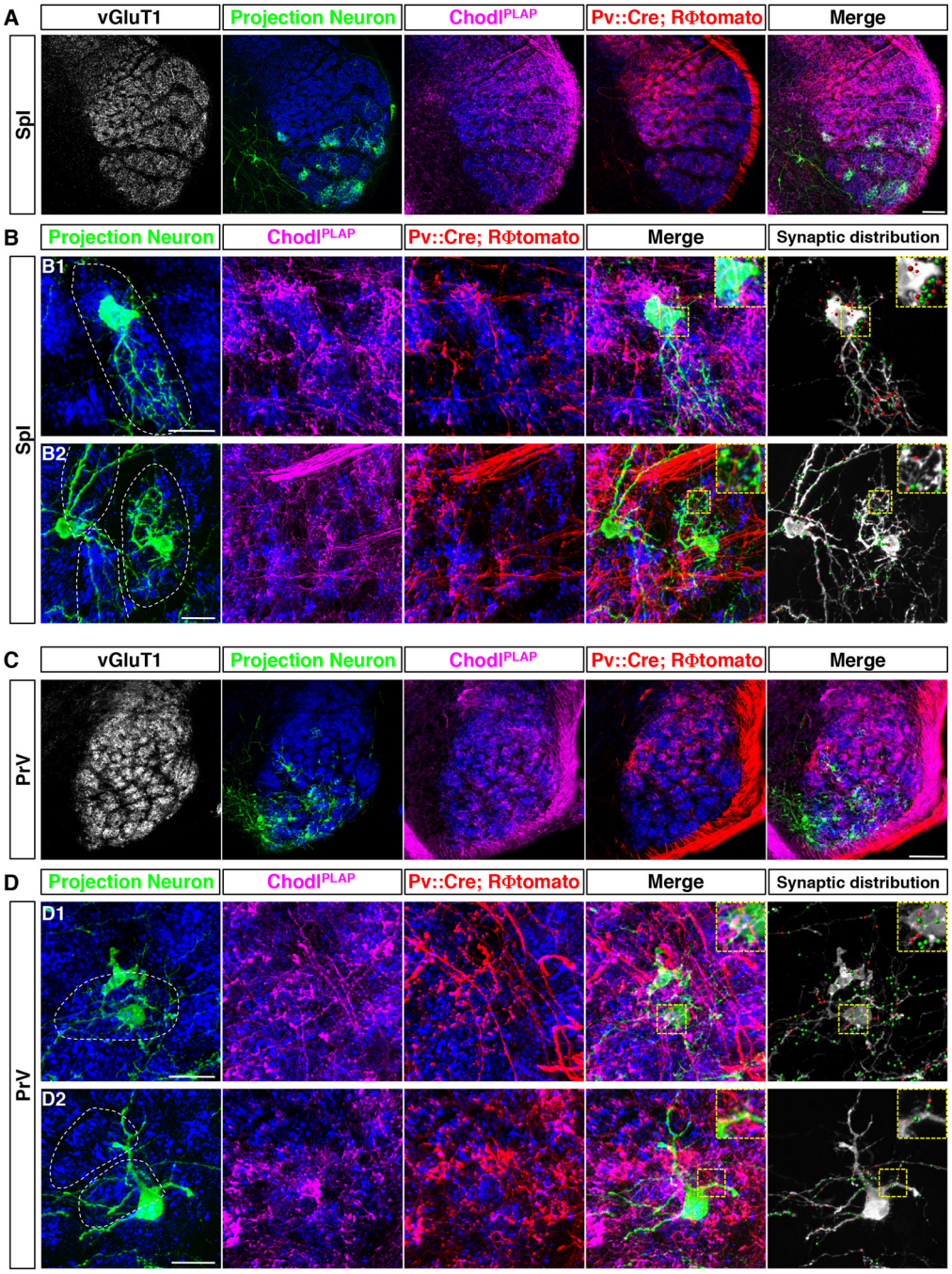

Fig. 4. Convergent RA and SA inputs onto brainstem projection neurons

(**A, C**) Representative low magnification images of the 4-color labeling experiments in SpI (**A**) or PrV (**C**) nucleus: vGluT1+ synaptic sites (grey or blue, synapses), projection neurons (green), RA-afferents (PLAP, magenta) and SA-afferents (tomato, red), from Pv::Cre; RΦtomato; Chodl^{PLAP} triple transgenic mice (P7) with ΔG-GFP-rabies virus injected into the thalamus.

(**B, D**) Tow representative high magnification images of the 4-color labeling experiments in SpI (**B**) or PrV (**D**) nucleus. White dash lines encircle the barrelette structure. Rightmost panels show synaptic terminals of SA-Merkel and RA-lanceolate-ending neurons onto the

labeled projection neurons. Red dots: SA- synapses. Green dots: RA- synapses. Insets: zoom of the yellow boxed region.
Scale bars: 100 μm (A, C), 20 μm (B, D).
See also Figure S5 and S6.

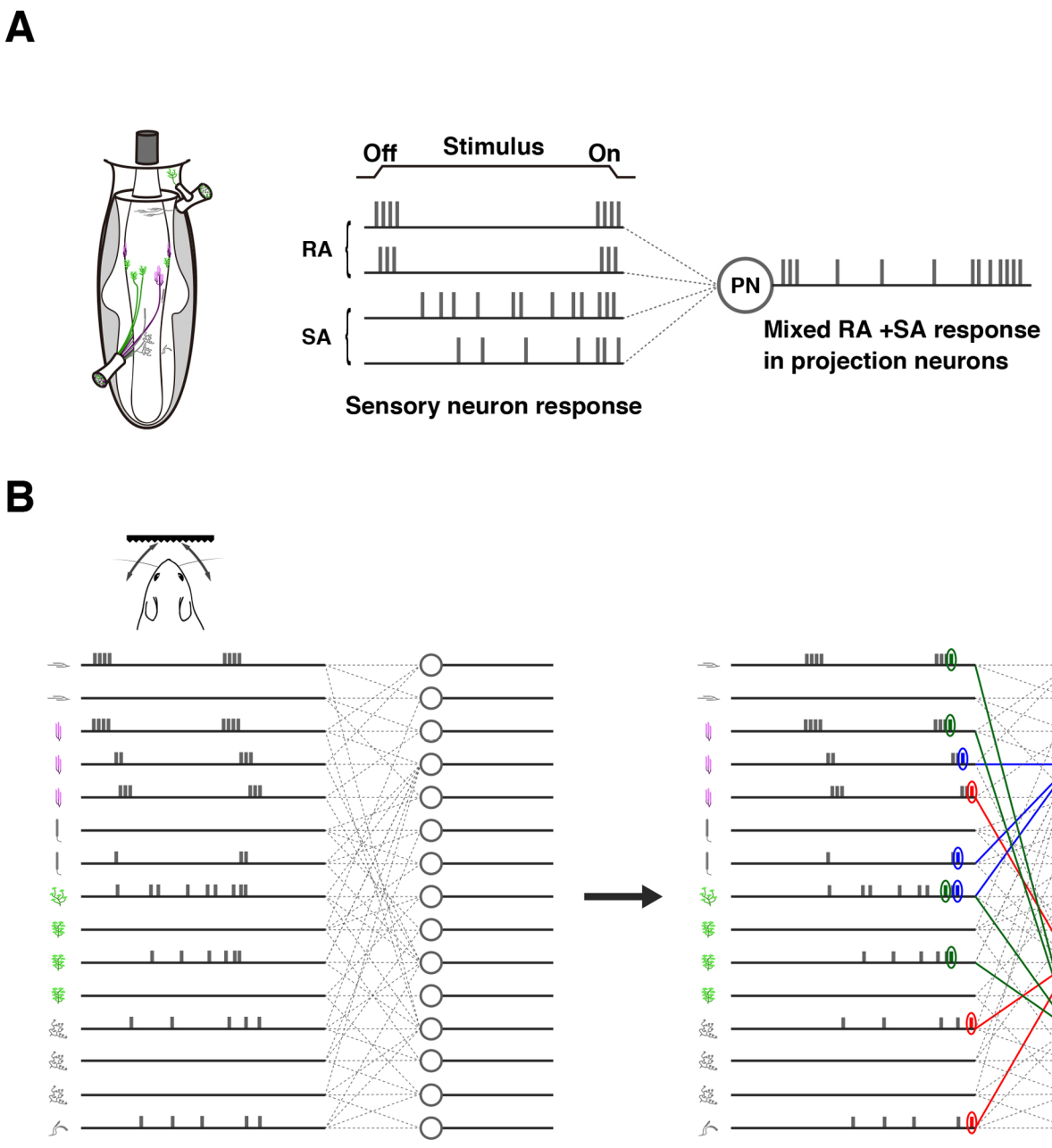

Fig. 5. Hypothetical model involving temporal coding of tactile information in the first relay station of the vibrissa sensory pathway

(**A**) A projection neuron (PN) receives convergent SA and RA inputs and thus shows mixed RA and SA responses.

(**B**) Hypothetical model: The sensory circuit from a single vibrissa to the brain has the one-to-many and many-to-one connectivity architecture. The individual neuronal spike and adaption patterns elicited by a touch stimulus are hypothetical on the model. We speculate that the spike-timing differences in sensory neurons in response to the touch stimulus and coincident detection of transiently synchronous spikes by PNs can result in a temporal code from the vibrissa column to encode the nature of tactile stimulus.